

Low Spin Polarization in Heavy-Metal–Ferromagnet Structures Detected Through Domain-Wall Motion by Synchronized Magnetic Field and Current

Xueying Zhang,^{1,2,3} Nicolas Vernier,³ Laurent Vila,⁴ Shaohua Yan,^{1,2} Zhiqiang Cao,^{1,2} Anni Cao,¹ Zilu Wang,¹ Wenlong Cai,^{1,2} Yang Liu,¹ Huaiwen Yang,^{1,2} Dafiné Ravelosona,³ and Weisheng Zhao^{1,2,*}

¹*Fert Beijing Institute, BDBC, School of Microelectronics, Beihang University, Beijing 100191, China*

²*Beihang-Goertek Joint Microelectronics Institute, Qingdao Research Institute, Beihang University, Qingdao 266000, China*

³*Centre for Nanoscience and Nanotechnology, University Paris-Saclay, 91405 Orsay, France*

⁴*University Grenoble Alpes, CEA, CNRS, Grenoble INP, INAC, SPINTEC, Grenoble 38400, France*

(Received 26 January 2019; revised manuscript received 20 April 2019; published 15 May 2019)

Co-Fe-B alloy is a very soft material, in which domain wall (DW) can be moved easily under a weak magnetic field. However, it is very difficult to move DWs in Ta/Co-Fe-B/MgO nanowires with interfacial perpendicular magnetic anisotropy through a spin-polarized current, and this limits the perspectives of racetrack memory driven by the current-in-plane mechanism. To investigate this phenomenon, we perform experiments of DW velocity measurement by applying magnetic field and current simultaneously. Working in the precessional regime, we are able to observe the effect of spin-polarized current, which allows the polarization rate of the charge carriers to be evaluated. An unexpected quite low spin-polarization rate down to 0.26 is obtained, which can explain the low efficiency of DW motion induced by the spin-polarized current. Possible reasons for this low rate, such as spin relaxation in the Ta layer, are analyzed.

DOI: 10.1103/PhysRevApplied.11.054041

I. INTRODUCTION

In computing technology, memories with larger storage densities, higher speed, and lower power consumption should be found. Magnetism provides interesting ways to obtain nonvolatile memories. One possibility is racetrack memory, in which moving domain walls (DWs) are used to store and transfer digital information [1,2]. However, to date, this strategy has not succeeded because moving DWs using only spin-polarized current seems to be more difficult than expected. Many materials have been studied [3], but pinning effects are often too strong to produce a reliable racetrack memory with them [4]. One of the promising materials is Ta/Co-Fe-B/MgO, in which the density of pinning sites seems very low, which enables movement of DWs using very low fields, as small as a few hundreds of μT [5–7]. However, although a quite good polarization rate of the charge carriers has been found in this material [8,9], very few authors have reported efficient movement in this material in zero fields using spin-polarized current only [10,11].

In addition, many physics problems in heavy-metal–ferromagnet structures [12–18], such as spin-transport properties and spin diffusion [19], must be understood.

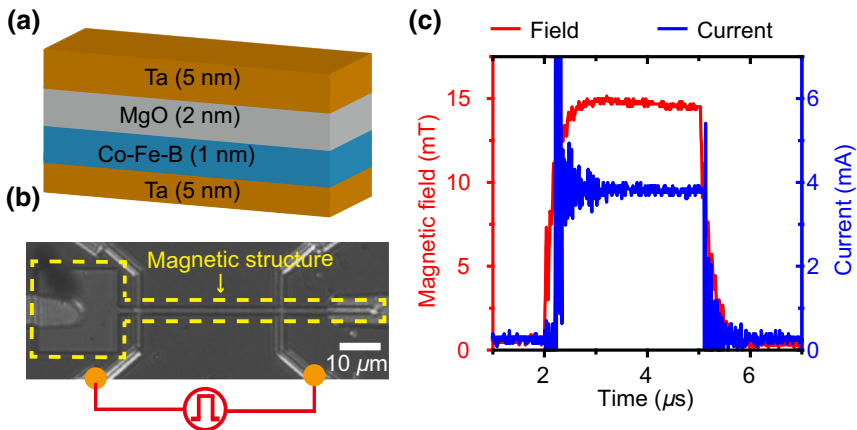
DW motion in Ta/Co-Fe-B/MgO provides a good model to perform this study.

To address these issues, we study DW motions induced by current and magnetic field in Ta/Co-Fe-B/MgO narrow wires. First, we present several attempts to move domain walls using spin-polarized current only in nanowires made of Ta/Co-Fe-B/MgO. These experiments result in a strange and nonconvincing behavior, which leads us to attempt another type of experiment: moving domain walls using both spin-polarized current and magnetic field. This way, we find the huge effect of the current. We deduce from this an effective spin-polarization ratio of the charge carriers. A possible explanation for this result is discussed.

II. EXPERIMENTS AND RESULTS

The sample studied is a Ta(5 nm)/Co₄₀Fe₄₀B₂₀(1 nm)/MgO(2 nm)/Ta(5 nm) multilayer stack with perpendicular anisotropy, as shown in Fig. 1(a). It is annealed at 300 °C for 2 h. In previous studies, samples prepared on the same wafer and with the same annealing condition as here have been experimentally studied and several properties of the samples have been characterized [5,20]: saturation magnetization is $M_S = 1.1 \times 10^6 \text{ A/m}$, effective perpendicular anisotropy energy is $K_{\text{eff}} = 2.2 \times 10^5 \text{ J/m}^3$, the damping

*weisheng.zhao@buaa.edu.cn



constant is $\alpha = 0.013$, and the DW width is estimated to be $\Delta = 10.7 \text{ nm}$. The Dzyaloshinskii-Moriya interaction (DMI) constant measured is less than 0.01 mJ/m^2 and the DW structure in this sample is identified to be of a pure Bloch type using magnetic microscopy based on a single nitrogen-vacancy defect in diamond [20].

The sample is patterned by conventional electron-beam lithography and ion-beam etching into $50\text{-}\mu\text{m}$ -long narrow wires connected with a $20 \mu\text{m} \times 20 \mu\text{m}$ square (nucleation pad). The width of the wire in these experiments is $1 \mu\text{m}$ or $1.5 \mu\text{m}$. Golden electrodes are added on the magnetic structure for electrical characterization. The structure of the device and the electrical test configuration are shown in Fig. 1(b).

In the experiments, a homemade Kerr microscope with a resolution of 500 nm is used to observe the DW behavior in the device. A high-voltage pulse generator is used to send current up to 15 A during a few μs in an 8-mm diameter coil. The small inductance of the mini coil, the large instantaneous output power, and the ultrafast speed of the power supply allow obtaining large and fast field pulses. For example, magnetic field pulses with an amplitude of 130 mT and a rise time of $1.9 \mu\text{s}$ have been produced by a coil having 120 turns. The large amplitude is able to nucleate a DW in the micron-sized device and the short duration avoids the complete magnetic reversal of the structure, thus a DW can be obtained after the pulse. With a 20-turn coil, field pulses with a rise time of 220 ns are obtained, so square-form field pulses of several microseconds are obtained. These pulses are synchronized with the electric current pulse, as shown in Fig. 1(c). A small delay between the field and the current is set, so that the magnetic field reaches its plateau when the current starts to flow in the wire.

In order to measure the DW velocity, first, after the DW nucleation, a Kerr image is acquired to locate the initial DW position. Then, a field (current, or both) pulse is applied and a second Kerr image is acquired to locate the final DW position. Finally, the DW-motion velocity

FIG. 1. (a) Stack structure of the studied sample. (b) Optical image of the tested device with a $1.5\text{-}\mu\text{m}$ -wide wire and the configuration of electric measurement. (c) Example of the synchronized electric current pulse and magnetic field pulse applied on the tested sample. These pulses are supervised by an oscilloscope.

is obtained by dividing the DW-motion distance by the duration of the field (or current) pulse.

First, we attempt to induce the DW motion by the current alone. However, no regular DW motion is observed even when the current density in the Ta/Co-Fe-B layer is increased to about $4.5 \times 10^{11} \text{ A/m}^2$, as shown in Figs. 2(a) and 2(b). Although a little DW motion in the direction of electron flow is observed, this motion is not reproducible. When the current density further increases, the DW-motion direction becomes stochastic: above a critical current density, DWs can also travel in the direction of current or opposite to this direction for the same pulse. The behavior of DWs is not reproducible and seems completely random. This is similar to the phenomena observed by Le Gall *et al.* [21].

In view of the difficulty of DW motion driven by current alone in this material, we begin to search for the regular and reproducible DW motions induced by the combined effects of the magnetic field and the electrical current. After DW nucleation, synchronized field pulses and current pulses are applied, all combinations of signs for the B_{\perp} component and for the current are checked. We find that, compared with DW motions induced by the magnetic field alone, the DW-motion velocity changes obviously when the current is introduced. In high fields, for which the precessional regime is reached, the motion is accelerated in the direction of the electrons, while it is slowed down when the DW motion is opposite to the direction of the electron flow, as shown in Fig. 3.

Velocities of DW motion with different current density and perpendicular field are measured systematically, as shown in Fig. 4(a). One can find that the DW velocity is obviously accelerated in the direction of electrons in the plateau (i.e., the DW motion when $\mu_0 H_{\perp} \geq 13 \text{ mT}$).

III. DISCUSSIONS

Theoretically, in a defect-free film, the field-induced DW motion begins with the steady-state regime at a low

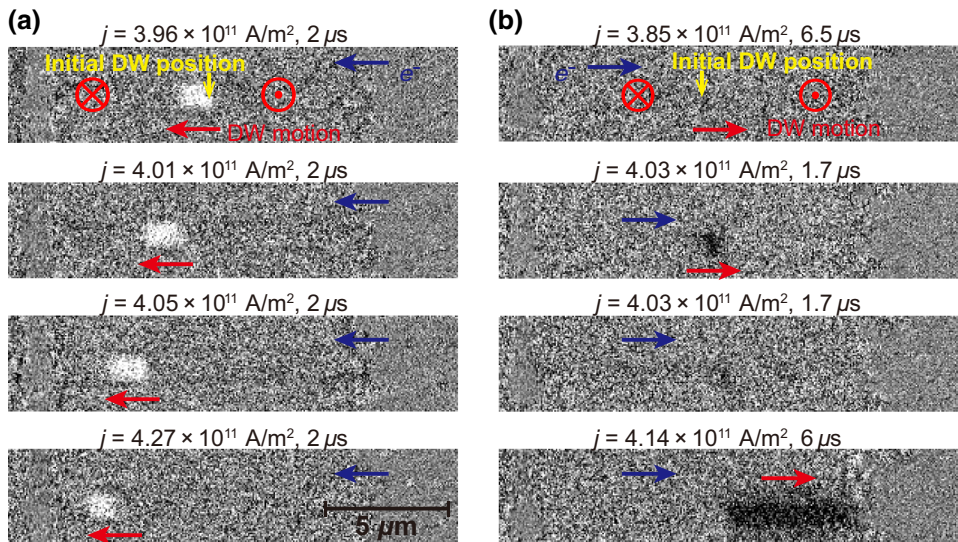


FIG. 2. (a) A series of DW motion to the left and (b) to the right, in a 1.0- μm -wide wire driven by successive current pulses. Each picture is obtained by making the difference between a picture taken before the pulse and a picture taken after the pulse. So, the contrast shows the change of magnetization, which has occurred during the pulse. Blue arrows indicate directions of electron flow, red arrows indicate the DW-motion directions, ⊙ and ⊗ indicate the magnetization directions.

applied field, during which velocities of DW increase linearly with the magnitude of applied fields [22]. As the applied field is further increased, the Walker breakdown is reached, and the DW starts to move in the precessional regime. The Walker breakdown field can be calculated as $H_W = \alpha M_S/2$ [22]. In the sample studied here, this field is estimated to be as low as 0.8 mT due to the low damping. Experimentally, this theoretical behavior is very difficult to observe [23]. Because of unavoidable defects in real samples, DW motion is dominated by pinning effects for low driving fields. Typically, DW moves in the creep [24–26] or depinning transition regime [27] when the driving force is lower or approximately equal to the pinning force. According to the field-induced DW-motion velocity measured on this device and the fitting with the creep law and depinning transition law, the creep and depinning transition regimes end at a field of 4 mT and about 13 mT, respectively (see Supplemental Material [28]). Obviously, the plateau of DW velocity obtained in Fig. 4(a) corresponds to the precessional regime

while the Walker breakdown is masked by the pinning effects.

The dynamic of DW driven by a magnetic field along the easy axis and the spin-transfer torque (STT) can be described by the following one-dimensional (1D) model [29,30]:

$$\dot{\varphi} + \frac{\alpha}{\Delta} \dot{q} = \gamma_0 H_Z + \xi \frac{\mu_B P}{e \Delta M_s} j_{\text{STT}}, \quad (1)$$

$$-\alpha \dot{\varphi} + \frac{\dot{q}}{\Delta} = \frac{\gamma_0 H_K}{2} + \sin 2\varphi \frac{\mu_B P}{e \Delta M_s} j_{\text{STT}}, \quad (2)$$

where q is the position of the DW, φ the angle between the magnetization at the center of the DW with respect to the longitudinal direction of the wire (azimuth angle), γ_0 the gyromagnetic ratio, ξ the nonadiabatic parameter, H_K the shape anisotropy field of DW, H_Z the applied field in the perpendicular direction, μ_B the Bohr magneton, e the electric charge, P the spin-polarization ratio, and j_{STT} the current density in the magnetic layer.

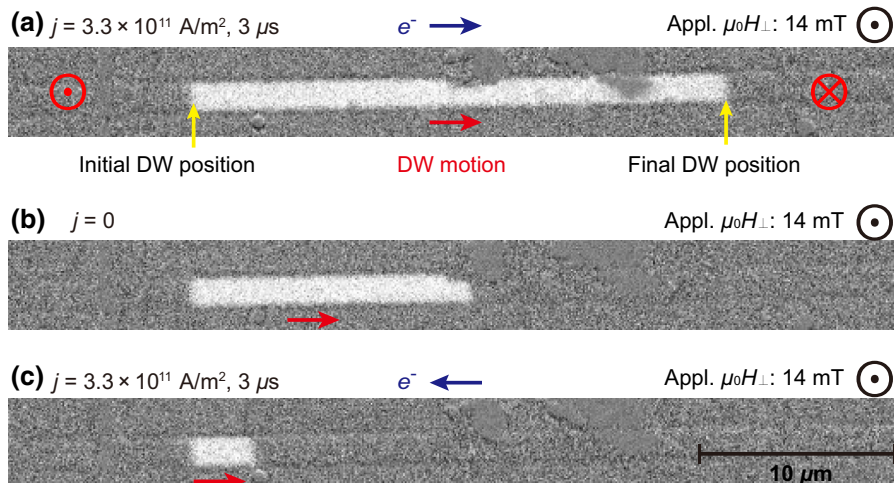


FIG. 3. DW motion driven by synchronized current and field pulse. The white contrast gives the DW-motion distance. Blue arrows indicate directions of electron flow, red arrows indicate the DW-motion directions, and ⊙ and ⊗ in red indicate the magnetization directions.

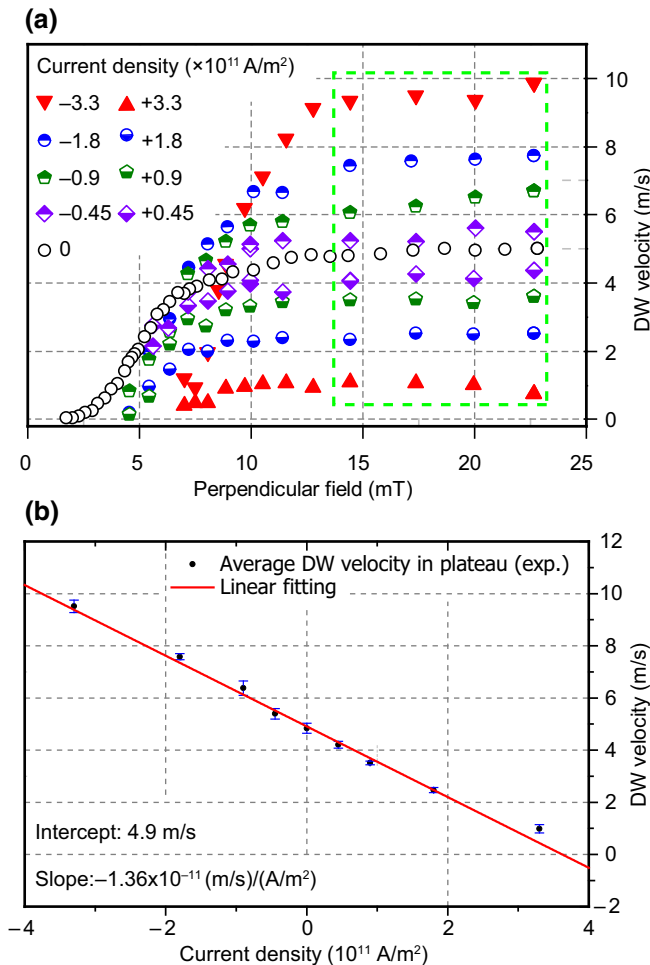


FIG. 4. (a) DW-motion velocities induced by different fields and current densities. Current flowing along the field-induced DW-motion direction is defined as positive. Velocities in the plateau, boxed by the dashed green line, correspond to the DW motion in the precessional regime. (b) Averaged velocities of DW motion shown in the plateau of (a) (enclosed in green). The error bar is taken as the standard deviation. The red line is a linear fitting on all these velocities. The current density in the Co-Fe-B layer is estimated using $\rho_{\text{CFB}} = 170 \mu\Omega \text{cm}$.

In the precessional regime, φ alternates from 0 to 2π , and $\sin \varphi = 0$ (the same for $\cos \varphi$ and $\sin 2\varphi$). In this case, the Slonczewski torque from the eventual spin Hall current arising from the sub-Ta layer is zero. Our observation is consistent with the fact that the DMI is very weak in this sample; if not, the DMI will fix the magnetization of the DW and no precession will occur at relatively low fields [31].

By assuming $\sin 2\varphi = 0$, we obtain

$$v_{\text{STT}+B} = v_{\text{STT}} + v_B, \quad (3)$$

with

$$v_{\text{STT}} = \frac{1 + \alpha\xi}{1 + \alpha^2} \times \frac{\mu_B P}{eM_s} j_{\text{STT}}. \quad (4)$$

In view that $\alpha \ll 1$, v_{STT} can be approximated by the spin drift velocity [30],

$$v_{\text{STT}} = \frac{\mu_B P}{eM_s} j_{\text{STT}}. \quad (5)$$

Now, let us return to the experimental results shown in Fig. 4(a). In the precessional mode, DW velocities remain stable in this range, we perform an average on the velocities [enclosed in the green dashed lines in Fig. 4(a)] for each current and plot the mean velocities as a function of the applied current, as shown in Fig. 4(b). A very good linear relationship between the DW velocity and the magnitude of the applied current is obtained, consistent with the above analysis [Eqs. (3)–(5)]. After a linear fitting, an intercept of 4.9 m/s and a slope $k = -1.36 \times 10^{-11} (\text{m/s})/(\text{A/m}^2)$ are obtained. Note that in this plot, we assume that the current density in each conductive layer is proportional to its conductivity, thus, the current density in the Co-Fe-B layer can be estimated with $j_{\text{STT}} = U/l\rho_{\text{CFB}}$, where U is the potential difference between the two terminals of the measured wire, l is the length of the wire, and ρ_{CFB} is the resistivity of Co-Fe-B. According to our experiments and the published literature [3,32–38] (see Supplemental Material [28]), $\rho_{\text{CFB}} = 170 \mu\Omega \text{cm}$ is used.

In fact, the relationship described in Eq. (3) has been observed in some experiment performed on materials with the in-plane anisotropy such as the permalloy [1,39,40] or on the $[\text{CoNi}]_n$ superlattice with perpendicular magnetic anisotropy [21]. In the linear relationship described in Fig. 4, the intercept corresponds to the DW velocity induced by the magnetic field alone and the slope represents the contribution from the current-induced motion. Based on this slope and the relationship described in Eq. (5), we obtain the effective polarization of Co-Fe-B in these experiments: $P = 0.26$.

The polarization ratio obtained by measuring the in-plane current-induced DW motion is much lower than the intrinsic spin-polarization ratio of Co-Fe-B measured through point-contact Andreev reflection (65%) [8], through superconducting tunneling spectroscopy (53%) [9,41,42] in the heavy-metal/Co-Fe-B/oxide layer structure or through spin absorption experiment on $\text{Co}_{60}\text{Fe}_{40}$ in lateral spin valves (48%) [19].

The low polarization measured through the STT-induced DW motion in Ta/Co-Fe-B/MgO structure may be caused by the following reasons. First, since the thickness of each layer in the studied stack has already decreased to the same dimension as the electrons mean free path of bulk metals (typically several nanometers for Co and Fe [43,44], 0.5–5 nm for β -Ta, and dozens of nanometers for bbc-Ta [45–47]), the scattering effect during the electron motions must be taken into consideration. These scatterings include the so-called sidewall-surface scattering (at the Co-Fe-B/MgO interface here), the grain boundaries

scattering in the Co-Fe-B and Ta layer [48], and the scattering caused by the roughness at the Ta/Co-Fe-B interface [49,50]. As a result, the conduction electrons interpenetrate between the Ta layer and the Co-Fe-B layer. Electrons scattered into the Ta layer will lose the specified spin polarization soon because of the short diffusion length (around 2 nm) of Ta [19]. While, the spin diffusion length for Co-Fe-B is estimated to be around 6 nm referring to the value of CoFe, larger than the Co-Fe-B-layer thickness [19]. In this case, the non-spin-polarized electrons scattered from the Ta layer effectively decrease the spin-polarization ratio of the whole Co-Fe-B layer in the studied scenario. Second, the spin current injected into the Co-Fe-B layer, or spin accumulation at the Ta/Co-Fe-B interface due to spin Hall and Rashba effects may also reduce the spin polarization of Co-Fe-B. It should be noticed that the above analysis is based on simplistic arguments. The electronic transport in ultrathin films is a very complex phenomenon, therefore theoretical input is needed to support these arguments and to reach more robust conclusions.

Note that we find that it is difficult to observe the DW motion driven by electric current alone in this structure. The low effective spin polarization for current flowing in the plane of Ta/Co-Fe-B may be one of the reasons to explain this difficulty. These explanations are consistent with a recent result: it is found that DWs could be moved quite easily in the same kind of sample if the thickness of Ta is reduced [10,11]. Indeed, in this case, electrons scattered from the Ta layer are reduced and we can expect a better spin-polarization rate of the charge carriers making the DW motion easier.

IV. CONCLUSION

In conclusion, the DW motion in Ta/Co-Fe-B/MgO narrow wire induced by the combined effect of magnetic field and electrical current is observed and measured with Kerr microscopy. In the precessional regime, the DW velocity is found to be the linear addition of the field-induced velocity and the spin-polarized current drift velocity. The spin polarization of the Co-Fe-B in this structure is extracted based on the dependence of the DW velocity on the current density, which is found to be much lower than the polarization in the case where current flows perpendicularly to the plane. This decay of spin polarization may be explained by the interpenetration of electrons between the heavy-metal and ferromagnet layers and the strong spin-orbit coupling in the heavy-metal layer. This result can explain the long-standing difficulty of the current-induced DW motion in similar structures.

ACKNOWLEDGMENTS

The authors gratefully acknowledge the National Natural Science Foundation of China (Grants No.

61627813 and No. 61571023), Programme of Introducing Talents of Discipline to Universities (Grant No. B16001), the National Key Technology Program of China 2017ZX01032101 and the China Scholarship Council.

-
- [1] S. S. P. Parkin, M. Hayashi, and L. Thomas, Magnetic domain-wall racetrack memory, *Science* **320**, 190 (2008).
 - [2] C. H. Marrows, Spin-polarised currents and magnetic domain walls, *Adv. Phys.* **54**, 585 (2005).
 - [3] J. Torrejon, J. Kim, J. Sinha, S. Mitani, M. Hayashi, M. Yamanouchi, and H. Ohno, Interface control of the magnetic chirality in CoFeB/MgO heterostructures with heavy-metal underlayers, *Nat. Commun.* **5**, 4655 (2014).
 - [4] T. Koyama, D. Chiba, K. Ueda, K. Kondou, H. Tanigawa, S. Fukami, T. Suzuki, N. Ohshima, N. Ishiwata, Y. Nakatani, K. Kobayashi, and T. Ono, Observation of the intrinsic pinning of a magnetic domain wall in a ferromagnetic nanowire, *Nat. Mater.* **10**, 194 (2011).
 - [5] C. Burrowes, N. Vernier, J.-P. Adam, L. Herrera Diez, K. Garcia, I. Barisic, G. Agnus, S. Eimer, J.-V. Kim, T. Devolder, A. Lamperti, R. Mantovan, B. Ockert, E. E. Fullerton, and D. Ravelosona, Low depinning fields in Ta-CoFeB-MgO ultrathin films with perpendicular magnetic anisotropy, *Appl. Phys. Lett.* **103**, 182401 (2013).
 - [6] X. Zhang, N. Vernier, W. Zhao, H. Yu, L. Vila, Y. Zhang, and D. Ravelosona, Direct Observation of Domain-Wall Surface Tension by Deflating or Inflating a Magnetic Bubble, *Phys. Rev. Appl.* **9**, 024032 (2018).
 - [7] X. Zhang, N. Vernier, W. Zhao, L. Vila, and D. Ravelosona, Extrinsic pinning of magnetic domain walls in CoFeB-MgO nanowires with perpendicular anisotropy, *AIP Adv.* **8**, 056307 (2018).
 - [8] S. X. Huang, T. Y. Chen, and C. L. Chien, Spin polarization of amorphous CoFeB determined by point-contact Andreev reflection, *Appl. Phys. Lett.* **92**, 242509 (2008).
 - [9] H. J. M. Swagten, P. V. Paluskar, R. Lavrijsen, J. T. Kohlhepp, and B. Koopmans, Tunneling spin polarization and annealing of Co₇₂Fe₂₀B₈, *J. Magn. Magn. Mater.* **310**, 2012 (2007).
 - [10] S. DuttaGupta, S. Fukami, B. Kuerbanjiang, H. Sato, F. Matsukura, V. K. Lazarov, and H. Ohno, Magnetic domain-wall creep driven by field and current in Ta/CoFeB/MgO, *AIP Adv.* **7**, 055918 (2017).
 - [11] S. DuttaGupta, S. Fukami, C. Zhang, H. Sato, M. Yamanouchi, F. Matsukura, and H. Ohno, Adiabatic spin-transfer-torque-induced domain wall creep in a magnetic metal, *Nat. Phys.* **12**, 333 (2016).
 - [12] A. Hrabec, N. A. Porter, A. Wells, M. J. Benitez, G. Burnell, S. McVitie, D. McGrouther, T. A. Moore, and C. H. Marrows, Measuring and tailoring the Dzyaloshinskii-Moriya interaction in perpendicularly magnetized thin films, *Phys. Rev. B* **90**, 020402(R) (2014).
 - [13] Y. Takeuchi, C. Zhang, A. Okada, H. Sato, S. Fukami, and H. Ohno, Spin-orbit torques in high-resistivity-W/CoFeB/MgO, *Appl. Phys. Lett.* **112**, 192408 (2018).

- [14] M. T. Rahman, R. K. Dumas, N. Eibagi, N. N. Shams, Y.-C. Wu, K. Liu, and C.-H. Lai, Controlling magnetization reversal in Co/Pt nanostructures with perpendicular anisotropy, *Appl. Phys. Lett.* **94**, 042507 (2009).
- [15] J. Kim, J. Sinha, M. Hayashi, M. Yamanouchi, S. Fukami, T. Suzuki, S. Mitani, and H. Ohno, Layer thickness dependence of the current-induced effective field vector in Ta|CoFeB|MgO, *Nat. Mater.* **12**, 240 (2013).
- [16] M. Bersweiler, E. C. I. Enobio, S. Fukami, H. Sato, and H. Ohno, An effect of capping-layer material on interfacial anisotropy and thermal stability factor of MgO/CoFeB/Ta/CoFeB/MgO/capping-layer structure, *Appl. Phys. Lett.* **113**, 172401 (2018).
- [17] G. Chen, S. P. Kang, C. Ophus, A. T. N'Diaye, H. Y. Kwon, R. T. Qiu, C. Won, K. Liu, Y. Wu, and A. K. Schmid, Out-of-plane chiral domain wall spin-structures in ultrathin in-plane magnets, *Nat. Commun.* **8**, 15302 (2017).
- [18] X. Zhang, W. Cai, X. Zhang, Z. Wang, Z. Li, Y. Zhang, K. Cao, N. Lei, W. Kang, Y. Zhang, H. Yu, Y. Zhou, and W. Zhao, Skyrmions in magnetic tunnel Junctions, *ACS Appl. Mater. Interfaces* **10**, 16887 (2018).
- [19] G. Zahnd, L. Vila, V. T. Pham, M. Cosset-Cheneau, W. Lim, A. Brenac, P. Laczkowski, A. Marty, and J. P. Attané, Spin diffusion length and polarization of ferromagnetic metals measured by the spin-absorption technique in lateral spin valves, *Phys. Rev. B* **98**, 174414 (2018).
- [20] J.-P. Tetienne, T. Hingant, L. J. Martínez, S. Rohart, A. Thiaville, L. H. Diez, K. Garcia, J.-P. Adam, J.-V. Kim, J.-F. Roch, I. M. Miron, G. Gaudin, L. Vila, B. Ocker, D. Ravelosona, and V. Jacques, The nature of domain walls in ultrathin ferromagnets revealed by scanning nanomagnetometry, *Nat. Commun.* **6**, 6733 (2015).
- [21] S. Le Gall, N. Vernier, F. Montaigne, A. Thiaville, J. Sampaio, D. Ravelosona, S. Mangin, S. Andrieu, and T. Hauet, Effect of spin transfer torque on domain wall motion regimes in [Co/Ni] superlattice wires, *Phys. Rev. B* **95**, 184419 (2017).
- [22] A. Mougin, M. Cormier, J. P. Adam, P. J. Metaxas, and J. Ferré, Domain wall mobility, stability and Walker breakdown in magnetic nanowires, *Europhys. Lett.* **78**, 57007 (2007).
- [23] G. S. D. Beach, C. Nistor, C. Knutson, M. Tsoi, and J. L. Erskine, Dynamics of field-driven domain-wall propagation in ferromagnetic nanowires, *Nat. Mater.* **4**, 741 (2005).
- [24] P. J. Metaxas, J. P. Jamet, A. Mougin, M. Cormier, J. Ferré, V. Baltz, B. Rodmacq, B. Dieny, and R. L. Stamps, Creep and Flow Regimes of Magnetic Domain-Wall Motion in Ultrathin Pt/Co/Pt Films with Perpendicular Anisotropy, *Phys. Rev. Lett.* **99**, 217208 (2007).
- [25] S. Lemerle, J. Ferré, C. Chappert, V. Mathet, T. Giamarchi, and P. Le Doussal, Domain Wall Creep in an Ising Ultrathin Magnetic Film, *Phys. Rev. Lett.* **80**, 849 (1998).
- [26] F. Cayssol, D. Ravelosona, C. Chappert, J. Ferré, and J. P. Jamet, Domain Wall Creep in Magnetic Wires, *Phys. Rev. Lett.* **92**, 107202 (2004).
- [27] R. Diaz Pardo, W. Savero Torres, A. B. Kolton, S. Bustingorry, and V. Jeudy, Universal depinning transition of domain walls in ultrathin ferromagnets, *Phys. Rev. B* **95**, 184434 (2017).
- [28] See Supplemental Material at <http://link.aps.org/supplemental/10.1103/PhysRevApplied.11.054041> for more detailed information about the magnetic field-induced domain wall motion in the creep regime, depinning transition regime, and precessional regime in this sample; for more detailed information about the estimation of the resistivity of Co-Fe-B thin film.
- [29] L. Thomas, M. Hayashi, X. Jiang, R. Moriya, C. Rettner, and S. S. P. Parkin, Oscillatory dependence of current-driven magnetic domain wall motion on current pulse length, *Nature* **443**, 197 (2006).
- [30] O. Boulle, G. Malinowski, and M. Kläui, Current-induced domain wall motion in nanoscale ferromagnetic elements, *Mater. Sci. Eng. R Reports* **72**, 159 (2011).
- [31] T. Ha Pham, J. Vogel, J. Sampaio, M. Vaňatka, J.-C. Rojas-Sánchez, M. Bonfim, D. S. Chaves, F. Choueikani, P. Ohresser, E. Otero, A. Thiaville, and S. Pizzini, Very large domain wall velocities in Pt/Co/GdOx and Pt/Co/Gd trilayers with Dzyaloshinskii-Moriya interaction, *Europhys. Lett.* **113**, 67001 (2016).
- [32] L. Liu, C.-F. Pai, Y. Li, H. W. Tseng, D. C. Ralph, and R. A. Buhrman, Spin-torque switching with the giant spin hall effect of tantalum, *Science* **336**, 555 (2012).
- [33] S. Cho, S.-H. C. Baek, K.-D. Lee, Y. Jo, and B.-G. Park, Large spin Hall magnetoresistance and its correlation to the spin-orbit torque in W/CoFeB/MgO structures, *Sci. Rep.* **5**, 14668 (2015).
- [34] I. Miccoli, F. Edler, H. Pfür, and C. Tegenkamp, The 100th anniversary of the four-point probe technique: the role of probe geometries in isotropic and anisotropic systems, *J. Phys. Condens. Matter* **27**, 223201 (2015).
- [35] M. Cormier, A. Mougin, J. Ferré, A. Thiaville, N. Charpentier, F. Piéchon, R. Weil, V. Baltz, and B. Rodmacq, Effect of electrical current pulses on domain walls in Pt/Co/Pt nanotracks with out-of-plane anisotropy: Spin transfer torque versus Joule heating, *Phys. Rev. B* **81**, 024407 (2010).
- [36] Y.-T. Chen and W. H. Hsieh, Thermal, magnetic, electric, and adhesive properties of amorphous Co₆₀Fe₂₀B₂₀ thin films, *J. Alloys Compd.* **552**, 283 (2013).
- [37] Y.-T. Chen and S. M. Xie, Magnetic and electric properties of amorphous Co₄₀Fe₄₀B₂₀ thin films, *J. Nanomater.* **2012**, 1 (2012).
- [38] W. Kettler, Electrical resistivity and thermopower of amorphous Fe_xCo_{80-x}B₂₀ alloys, *J. Appl. Phys.* **53**, 8248 (1982).
- [39] G. S. D. Beach, C. Knutson, C. Nistor, M. Tsoi, and J. L. Erskine, Nonlinear Domain-Wall Velocity Enhancement by Spin-Polarized Electric Current, *Phys. Rev. Lett.* **97**, 057203 (2006).
- [40] M. Hayashi, L. Thomas, Y. B. Bazaliy, C. Rettner, R. Moriya, X. Jiang, and S. S. P. Parkin, Influence of Current on Field-Driven Domain Wall Motion in Permalloy Nanowires from Time Resolved Measurements of Anisotropic Magnetoresistance, *Phys. Rev. Lett.* **96**, 197207 (2006).
- [41] P. V. Paluskar, J. T. Kohlhepp, H. J. M. Swagten, and B. Koopmans, Co₇₂Fe₂₀B₈: Structure, magnetism, and tunneling spin polarization, *J. Appl. Phys.* **99**, 08E503 (2006).

- [42] P. V. Paluskar, J. T. Kohlhepp, H. J. M. Swagten, B. Koopmans, R. Wolters, H. Boeve, and E. Snoeck, Influence of interface structure on the tunnelling spin polarization of CoFeB alloys, *J. Phys. D: Appl. Phys.* **40**, 1234 (2007).
- [43] J. Hong and D. L. Mills, Spin dependence of the inelastic electron mean free path in Fe and Ni: Explicit calculations and implications, *Phys. Rev. B* **62**, 5589 (2000).
- [44] B. A. Gurney, V. S. Speriosu, J.-P. Nozieres, H. Lefakis, D. R. Wilhoit, and O. U. Need, Direct Measurement of Spin-Dependent Conduction-Electron Mean Free Paths in Ferromagnetic Metals, *Phys. Rev. Lett.* **71**, 4023 (1993).
- [45] G. Allen, S. Manipatruni, D. E. Nikonov, M. Doczy, and I. A. Young, Experimental demonstration of the coexistence of spin Hall and Rashba effects in β -tantalum/ferromagnet bilayers, *Phys. Rev. B* **91**, 144412 (2015).
- [46] E. Montoya, P. Omelchenko, C. Coutts, N. R. Lee-Hone, R. Hübner, D. Broun, B. Heinrich, and E. Girt, Spin transport in tantalum studied using magnetic single and double layers, *Phys. Rev. B* **94**, 054416 (2016).
- [47] D. Guan, Electron Mean Free Path in Epitaxial Ta(001) Layers, Rensselaer Polytechnic Institute, 2013. [<http://adsabs.harvard.edu/abs/2013PhDT.....68G>]
- [48] C. Huang, Y. Feng, X. Zhang, J. Li, and G. Wang, Electron mean free path model for rectangular nanowire, nanofilm and nanoparticle, *Phys. B Condens. Matter* **438**, 17 (2014).
- [49] D. J. Keavney, S.-K. Park, C. M. Falco, and J. M. Slaughter, Specular and diffuse electron scattering at interfaces in metal spin-valve structures, *J. Appl. Phys.* **86**, 476 (1999).
- [50] A. M. Zhang, H. L. Cai, and X. S. Wu, Spin dependence scattering and spin-flip effect on the current-in-plane transport behavior in NiO-based-spin valve, *Phys. Status Solidi Basic Res.* **247**, 329 (2010).